Title: Role of Induction Time on Carbon Dioxide and Methane Gas Hydrate Kinetics

Jean-Sébastien Renault-Crispo[1], Phillip Servio[1,]*

[1] Department of Chemical Engineering, McGill University, Montréal, Québec Canada.

* Corresponding author's email: phillip.servio@mcgill.ca

Tel.:+15143981026;

fax:+15143986678.

Postal address:

Room 3060, Wong Building

3610 University Street,

Montréal, Québec,

Canada, H3A 0C5

Abstract

This study showed a significant variability in gas consumption rate values during gas hydrate growth at a same experimental condition for a specific experimental setup. This is important since many studies report a singular gas consumption rate or no associated statistics. Carbon dioxide hydrate gas consumption rates had of coefficient of variation of 2.7% for 204 kPa, 9.7% for 317 kPa and 9.6% for 435 kPa driving forces. The gas consumption rates decreased with increasing induction time following a first-order response. A high induction time resulted in a higher bulk liquid temperature increase meaning a greater amount of initial carbon dioxide hydrates formed. Methane hydrates did not exhibit the same behaviour of gas consumption rate with induction time. Variations in methane gas consumption rates were 4.8% for 698 kPa and 2.4% for 1564 kPa driving forces. A regression of metastable dissolution during these kinetic experiments demonstrated that the liquid mole fraction limit increased with increasing driving force. The dissolution time constant decreased with increasing mixing rate. Finally, the maximum experimental liquid mole fraction supersaturation achieved during all experiments was 75 times smaller than the thermodynamically predicted spinodal limit.

Keywords

Gas hydrate; Induction time; Gas consumption rate; Hydrate kinetic; Hydrate dissolution

1 Introduction

Gas hydrates are non-stoichiometric crystalline compounds that form when a gas molecule is encapsulated by water molecules at relatively low temperatures and high pressures. Suitable guest molecules are mostly determined by size and stabilize the crystal lattice of hydrogen-bonded water molecules through weak van der Waals forces [1]. There are over 180 different molecules that form hydrates, with the most notable being methane and carbon dioxide [2]. Until the 1930's, hydrates remained mainly of academic interest until industrial research was spurred by the discovery of hydrates blocking natural gas transmission lines [3]. To this day, this problem of blockages remains quite significant and costly, as can be seen in the complications with the BP oil spills in the Gulf of Mexico that were due to a large volume of hydrates formed [4]. Another turning point in the field was the discovery of *in situ* natural gas hydrates in the Siberian permafrost [5]. Recently, various applications using hydrates have been proposed such as gas transportation, storage and separation [6-8]. Carbon dioxide sequestration in hydrate form has been studied as a mean to mitigate global warming [9, 10]. Dashti et al. provided a comprehensive study on the recent advances in gas hydrate-based CO_2 capture [11]. Slow and unpredictable formation kinetics and the lack of scalability studies have prevented larger scale development of these proposed technologies [7, 12].

Numerous studies have been performed to investigate the kinetics of gas hydrate formation in stirred tank crystallizers. These studies make use of the gas consumption rate to model the system and calculate the reaction rate constant. The pioneering publication by Vysniauskas and Bishnoi [13, 14] discussed the kinetics of methane and ethane hydrate formation. They assumed an Arrhenius-type function of temperature for the reaction rate kinetics. More recently, Bergeron and Servio [15-18] developed a model, shown in Equation 1, for hydrate growth in stirred tank reactors that focuses on the liquid phase, eliminating the need to calculate the mass transfer at the gas-liquid interface.

$$\frac{dn}{dt} = \frac{V_L \rho_w \left(x^L - x^{HL}\right)}{MW_w \, 1/(\pi \mu_2 k_r)} \tag{1}$$

where $\frac{dn}{dt}$ is the amount of moles consumed over time after the onset of growth, also called the gas consumption rate, V_L is the liquid volume in the reactor, ρ_w and MW_w are respectively the mass density and molecular weight of the liquid water at reactor conditions. The driving force for growth is the difference between the mole fraction of the hydrate-forming gas in the bulk liquid (x^L) and its solubility under hydrate-liquid equilibrium (x^{HL}). The second moment, μ_2, is a representation of the hydrate particle size. The last variable and what these models aim to predict is the intrinsic reaction rate constant k_r. In literature, the intrinsic reaction rate predictions vary by a few orders of magnitude for similar systems [15, 17, 19]. This discrepancy can be attributed to different reactor geometries, mixing rates, as well as error in measuring particle size, liquid mole fraction or gas consumption rates. Some reports used the initial gas consumption rate (e.g. first 15 minutes of growth) [15-17] while others utilized the gas consumption rate after up to 10 hours of growth [19]. Hence, the gas consumption rate can be significantly different for each experimental setup depending on the geometry of the reactor vessel, the speed of mixing, the amount of liquid present and the method of selecting the rate.

A molar gas consumption curve of hydrate formation and growth for a stirred reactor is presented in Figure 1. The process can be divided into three steps. The first step involves the dissolution of the hydrate-forming gas into the liquid phase until the liquid mole fraction reaches the point of three-phase equilibrium at the experimental temperature. As seen in Figure 1, this occurs at time t_{eq} where n_{eq} moles have been dissolved. The next step is the induction step, and is characterized by the liquid phase being supersaturated with the hydrate-forming gas. This occurs because the pressure is above the three-phase equilibrium pressure, enabling the formation of a new phase. Due to the stochastic nature of nucleation, gas hydrates can form at any time during this metastable induction period [1]. Small hydrate nuclei continuously form and dissociate until a critical radius size is reached where hydrate growth is energetically favourable [1]. This is denoted by the induction time t_{ind} and marks the start of the hydrate growth step [20]. A bulk liquid temperature spike, ΔT, from exothermic solidification, and an increase in opacity of the liquid are two indicators of the nucleation of hydrates in the reactor. Hydrate former gas consumption generally increases linearly over time at the early stage of growth.

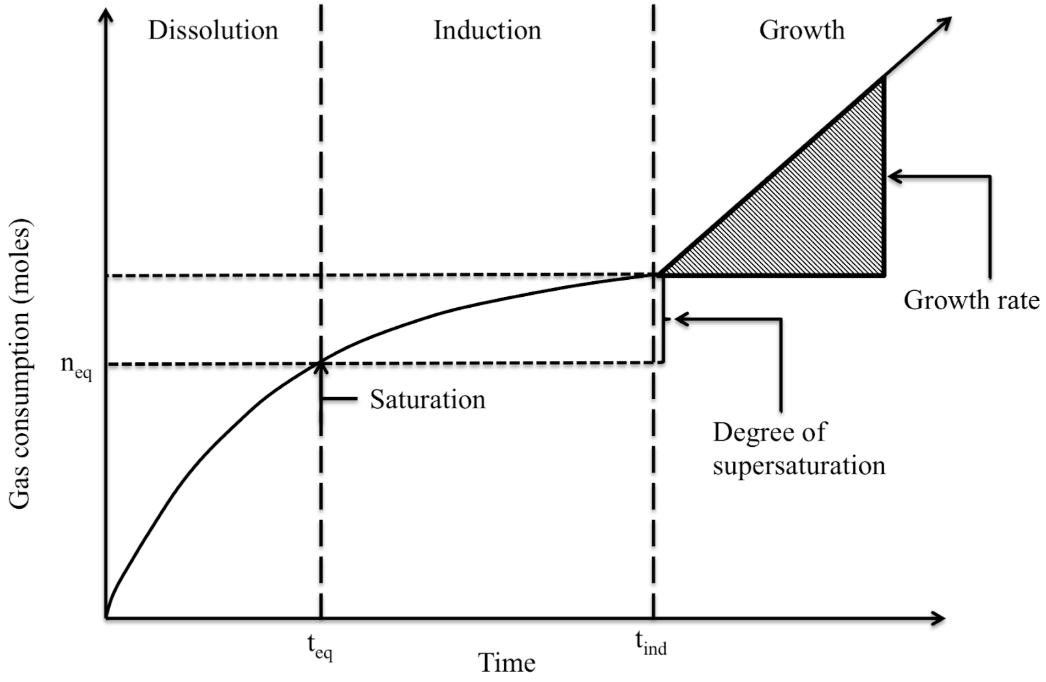

Figure 1: Simplified hydrate growth curve of gas consumption over time.

The dissolution and induction phases can be modeled together by applying dissolution kinetics. A first-order kinetic rate model is usually used to fit the data [21, 22] and can be seen in Equation 2.

$$n = n_{liq}\left(1 - e^{-\frac{t}{\tau}}\right) \tag{2}$$

where n_{liq} is the hypothetical maximum liquid moles dissolved if hydrates would not form and τ is the time constant used to designate the point in time where 63.2% of the n_{liq} is reached. A reduction of τ would thus indicate an increase in rate of dissolution. With a metastable system, the dissolution can only be fitted up to the growth phase since the presence of hydrates changes the gas consumption dynamics completely. It follows that the mole fraction of the hydrate forming gas in the liquid phase can also contribute to the understanding of kinetics. Bergeron and Servio [18] demonstrated that the mole fraction of the gas hydrate former in the bulk liquid phase during growth remained greater than its two-phase hydrate-liquid equilibrium value.

Although many studies have considered modeling and quantifying gas hydrate growth kinetics, the effect of induction time on the gas consumption rates has not been reported or even mentioned to the knowledge of the authors. It is critical to accurately determine the gas consumption rate in order to properly compare kinetic performances of different additives, especially when these gas consumption rates are compared directly or used to calculate the intrinsic kinetic rate. This study could also contribute to various industrial applications where time is a factor; hence rapid dissolution and short induction time are essential to reducing cost and improving efficiency. The liquid mole fractions of the gas hydrate former during dissolution are also investigated to provided further insights on the complete kinetic process.

2 Experimental

2.1 Experimental Setup

A detailed description of the experimental setup and procedure can be found in a previous report [23]. A simplified diagram of the experimental setup is shown in Figure 2. It consists of a 600 mL reactor made of 316 stainless steel with a pressure rating of 20 MPa submerged in a temperature controlled 20% ethylene glycol-water bath. The reactor is equipped with a MM-D06 magnetic stirrer from Pressure Products Industries with a standard magnetic stir bar with spinning ring from Cole Parmer. The reactor is connected to a reservoir gas tank through a Baumann 51000 control valve that keeps the pressure constant during kinetic experiments. For increase in accuracy, the control valve is regulated with the difference in pressure between the reactor bias gas tank and the reactor. The absolute pressures are monitored using Rosemount pressure transducers configured to a span of 0-14 MPa while the differential pressure transducers are configured to a span of 0-2 MPa, both with an accuracy of 0.065% of the given span. The system temperatures are recorded with RTD probes from Omega with accuracy of 0.1 K. All pressure and temperature readings are sent to a computer through a National Instrument data acquisition system. Liquid samples are removed from the reactor through a sampling port. A digital gasometer from Chandler Engineering is used to measure the amount of gas evolved from the liquid when the sample is left to equilibrate at room temperature and atmospheric pressure. All gases used were obtained from MEGS Inc., and included ultra-high purity methane gas (99.99%) and carbon dioxide gas (99.995%). The water was treated in-house by reverse-osmosis with a 0.22 μm filter having a conductivity of 10 μS and total organic content < 10 ppm.

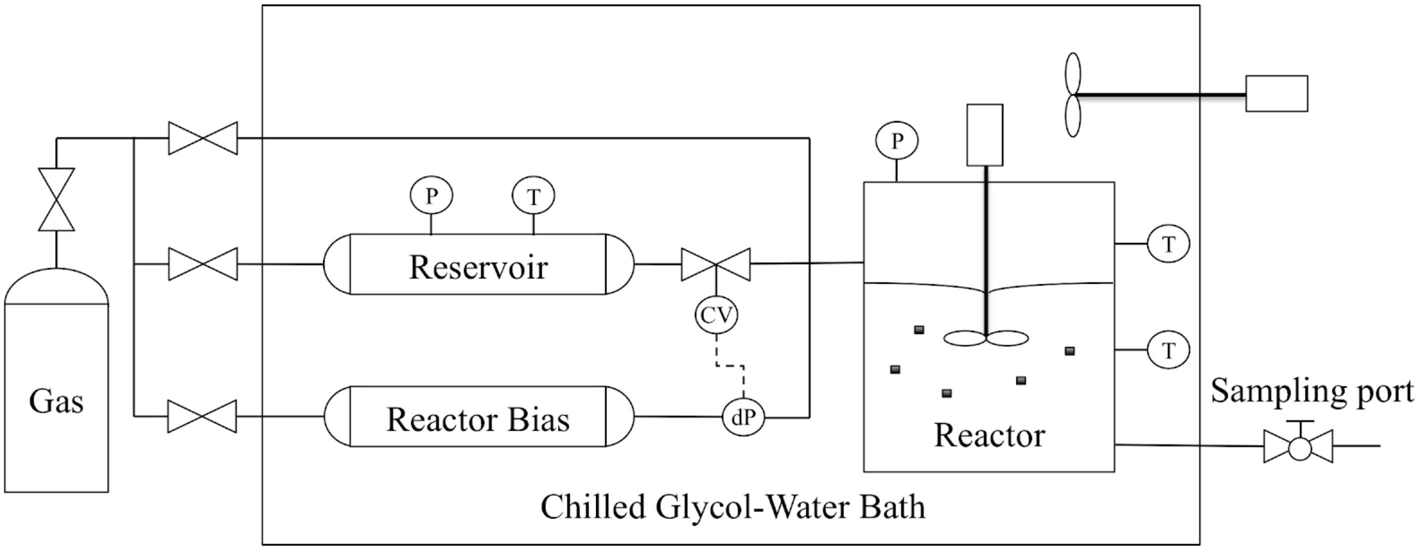

Figure 2: Schematic of the experimental setup used in all experiments.

2.2 Kinetic Experiments

Initially, the reactor was rinsed three times with 360 mL of water. Then, it was loaded with 240 mL of RO water. All kinetic experiments were performed with the same 240 mL of water to ensure the hydrodynamics were consistent across all experiments. The temperature of the bath was set to 2 °C for all experiments. The temperature was always kept at 2 °C and it was the pressure that was varied to provide the driving force for hydrate formation. Following water injection, the reactor gas was purged three times by pressurizing to 1100 kPa and then de-pressurizing to 110 kPa. Once thermal equilibrium was reached in the liquid, the reactor was pressurized to the desired pressure for the run based on the driving force. This driving force can be interpreted as either a temperature subcooling or a pressure driving force when compared to the three-phase equilibrium line. The reservoir and reactor bias gas tanks were pressurized to 1000 kPa above the reactor value to provide a differential pressure for gas transfer during the run. When the temperature stabilizes, the data acquisition system and control valve were turned on, and the stirrer was started. Once nucleated, the hydrates were allowed to grow for at least 300 seconds before the data acquisition system and control valve were turned off. 300 seconds was chosen to calculate the gas consumption rate as it was considered sufficient time to fit a linear slope but not too long so that the hydrodynamics would be changed by the presence of solids in the reactor. The system was subsequently brought down to 110 kPa for the hydrates to dissociate. Once all hydrates were dissociated, the reactor pressure was set to the initial pressure and the experiment was repeated. The moles consumed were calculated from the temperature and pressure data of the reservoir using the Trebble-Bishnoi equation of state [24, 25]. The gas consumption rate was calculated from the slope of moles consumed over time for the first 300 seconds of hydrate growth. The temperature spike ΔT was calculated from the difference between the highest temperature after nucleation and the average temperature before nucleation. The liquid mole fraction was calculated from the amount of moles consumed before hydrate formation accounting for the gas dissolved at the start of the run when reactor was at 110 kPa. The pressure slightly above atmospheric was to prevent gases from the atmosphere to enter the system.

2.3 Mole Fraction Experiments

An analytical flash technique, similar to the one used by Gaudette and Servio [26], was employed to calculate the mole fraction of methane in the bulk liquid during the dissolution and growth steps. The reactor was loaded with 360 mL to allow for multiple removals of liquid samples. Three sample vessels were evacuated and cooled to the experimental temperature prior to sample extraction. They were also weighed before and after the sample was collected. Prior to the removal of a sample, the stirrer was turned off to avoid having hydrates or air bubbles enter the sample vessel. The liquid from the reactor was extracted into the three sample vessels. Through the use of a gasometer, the content of the sample vessel was brought to atmospheric pressure and room temperature. The mole fraction was determined from the volume of gas released when exposed to atmospheric conditions, as shown in Bergeron et al. [15].

3 Results and Discussion

3.1 Carbon Dioxide Hydrate Kinetics

3.1.1 Effect of Driving Force

For the carbon dioxide-water gas hydrate system, experiments were completed at three different driving force presented in Table 1. Mixing speed and temperature in these experiments were kept constant at 560 rpm and 2 °C respectively.

Table 1: Three different driving force conditions for CO_2 hydrate kinetic experiments.

Temperature (°C)	Pressure (kPa)	Temperature subcooling (°C)	Pressure driving force (kPa)	Mixer speed (rpm)
2	1778	1	204	560
2	1891	1.5	317	560
2	2009	2	435	560

The dependency of gas consumption rate on induction time can be observed in Figure 3. Average induction times are 1077 seconds for 435 kPa driving force, 1692 seconds for 317 kPa driving force and 3635 seconds for 204 kPa driving force. As expected, average induction time decreases with increasing driving force [27]. More significantly, shorter induction times relate to higher gas consumption rates at a given temperature. Looking at the 317 kPa driving force runs, as induction time increases, the gas consumption rate eventually decreases to what is expected to be a plateau. Unfortunately, since induction time is stochastic, not many experimental points were collected in this plateau region of long induction times. At 204 kPa driving force, the coefficient of variance is 2.7% (average of 5.13E-5 mol/s with standard deviation of 1.4E-6 mol/s) compared to 9.7% (average of 6.28E-5 mol/s with standard deviation of 6.1E-6 mol/s) for 317 kPa driving force and 9.6% (5.13E-5 average of mol/s and standard deviation of 4.9E-6 mol/s) for 435 kPa driving force. For the two highest driving forces, there is a significant variation considering the experiments were conducted at the same conditions, namely 2 °C and 1891 kPa. According to Equation 1 and assuming other parameters are constant, this means that the predicted intrinsic reaction rate constant would also vary by the same amount as the gas consumption rate, which leads to error in its calculation since the intrinsic reaction rate is only a function of temperature in the system investigated. This result highlights the issue of solely reporting the gas consumption rate or intrinsic kinetic rate for systems where this trend is present since there could be a large variability in the results. Hence, the need for replicates and adequate statistical analysis are extremely important when reporting hydrate kinetics.

However, the gas consumption rate is not significantly affected by the induction time at the lowest driving force. This can be explained by the fact that it has longer periods for dissolution into the liquid and liquid mole fraction limit is lower due to the smaller pressure. At long induction times, the dissolution process is nearly completed and the liquid is close to its liquid mole fraction limit at a specific condition. In this case, it is possible to decouple the growth and dissolution phase and define our gas consumption rate as the actual hydrate growth rate, meaning that all the gas going into the liquid is for hydrate growth. At long induction times, the 317 and 435 kPa driving forces would probably also exhibit reproducible gas consumption rates. However, long induction times are difficult to achieve because of the elevated pressure conditions and overall driving forces for nucleation. This is a consistent statement with Herri et al. [28] who observed an inversely proportional trend between induction time and driving force. At short induction time, it was impossible to decouple dissolution kinetics and hydrate growth rates and this is the reason gas consumption rates are used throughout the paper. The presence of hydrates significantly affects the dissolution dynamics making it unreasonable to use the dissolution model from before hydrate formation to represent the dissolution during growth.

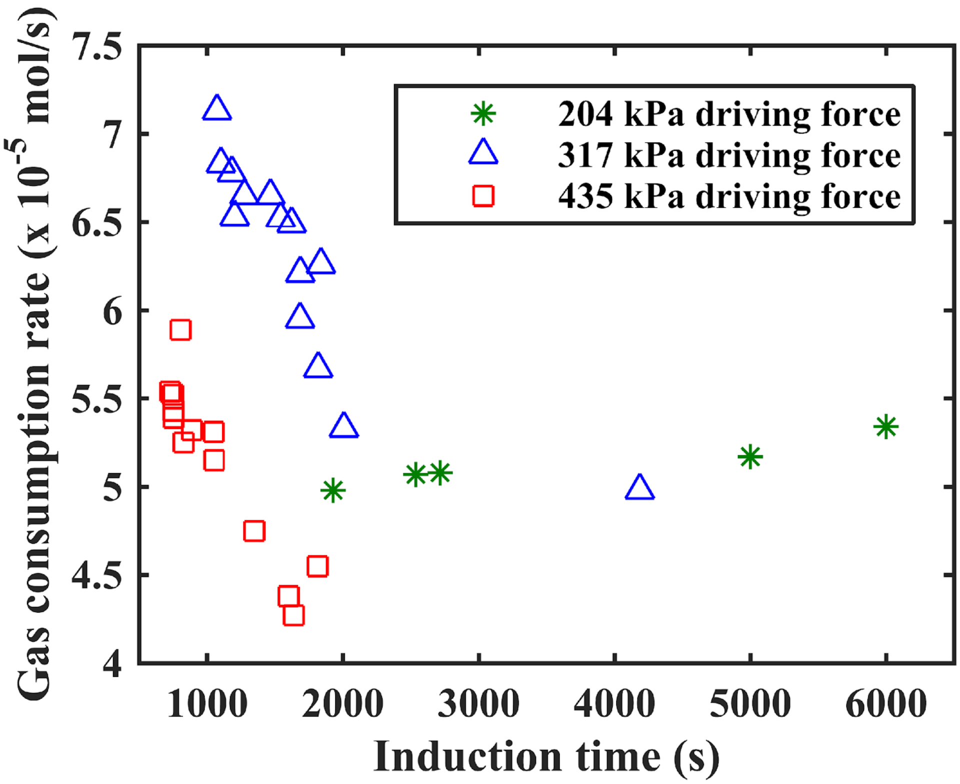

Figure 3: Gas consumption rate versus induction time for 3 different driving forces in a CO_2-water gas hydrate system: * 204 kPa, △ 317 kPa, □ 435 kPa.

As shown by Figure 3, the precise moment in the induction phase when the gas hydrates nucleate can be very important for characterizing the ensuing gas consumption rate. Figure 4 shows the change in temperature of the bulk liquid at hydrate formation for different induction times. The dissolution phase of the hydrate formation process is extremely reproducible for a given driving force at a fixed temperature. The dissolution section of the curves only varies when the experimental conditions do. In other words, the total amount of gas consumed at a specific induction time will always be the same before hydrate nucleation if the experimental conditions are consistent. This total gas consumed is directly related to the initial amount of gas hydrates formed at the induction time. The initial amount of gas hydrates formed at nucleation can also be linked to a bulk temperature spike because this process is exothermic. Hence, the more initial hydrates formed, the greater the temperature spike. This explains the increasing trend with induction time that is evident in Figure 4. Furthermore, this trend is present as a first-order response as it seems to follow dissolution kinetics. Greater driving forces show higher temperature spikes because of the enhanced dissolution rates and greater levels of liquid mole fraction limit.

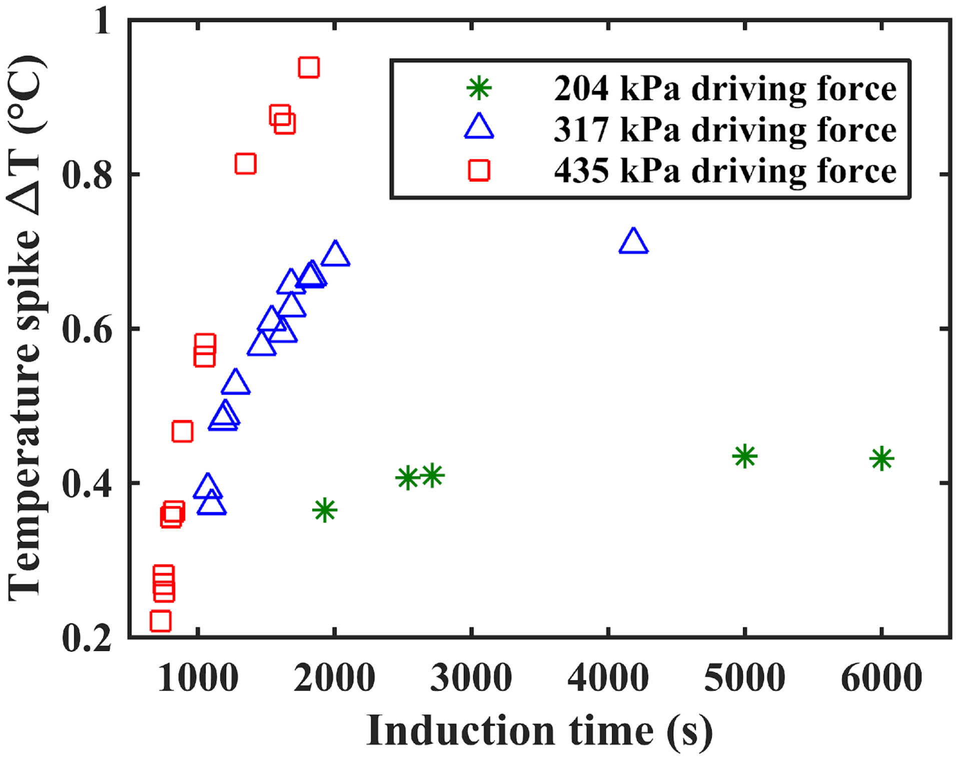

Figure 4: Temperature spike versus induction time for 3 different driving forces in a CO_2-water gas hydrate system: * 204 kPa, △ 317 kPa, □ 435 kPa.

This temperature spike dependency can help explain why gas consumption rates decreases with increasing induction times as observed in Figure 3. The presence of a greater initial amount of gas hydrates changes the hydrodynamics of the system. The mixing could be less efficient with the presence of more initial hydrates in the reactor and this also affects the gas-liquid mass transfer of the system. Additionally, having a greater temperature increase of the bulk liquid lowers the driving force for hydrate growth and slows down the kinetics. These two arguments are a suitable explanation to the reason why the gas consumption rate decreases with increasing induction time.

To further investigate this effect, one specific experiment was selected and the instantaneous gas consumption rates and bulk liquid temperature were compared over time during hydrate growth to see their relationship. The results can be observed in Figure 5. The instantaneous gas consumption rate is the slope of gas consumed over a duration of 10 seconds to eliminate the effect of noise in the growth rate calculation. The instantaneous gas consumption rate decreases slowly over time, following a similar decreasing trend than the bulk liquid temperature over time. This growth rate goes below the average gas consumption rate reported throughout this paper after approximately 600 seconds for this experimental run. The decrease can be mainly attributed to the bulk liquid temperature decrease but also to change in hydrodynamics (e.g. change in viscosity of the liquid). This is the reason why the initial growth rate of the first 300 seconds was selected in this report to decouple it from the other effects on the growth rate. It is important to keep in mind that the bulk liquid temperature is not simply a linear function of consumption rate as can be concluded from the higher temperature spikes of the 2 °C driving force compared to 1.5 °C but the lower gas consumption rates as seen in Figure 3 and Figure 4.

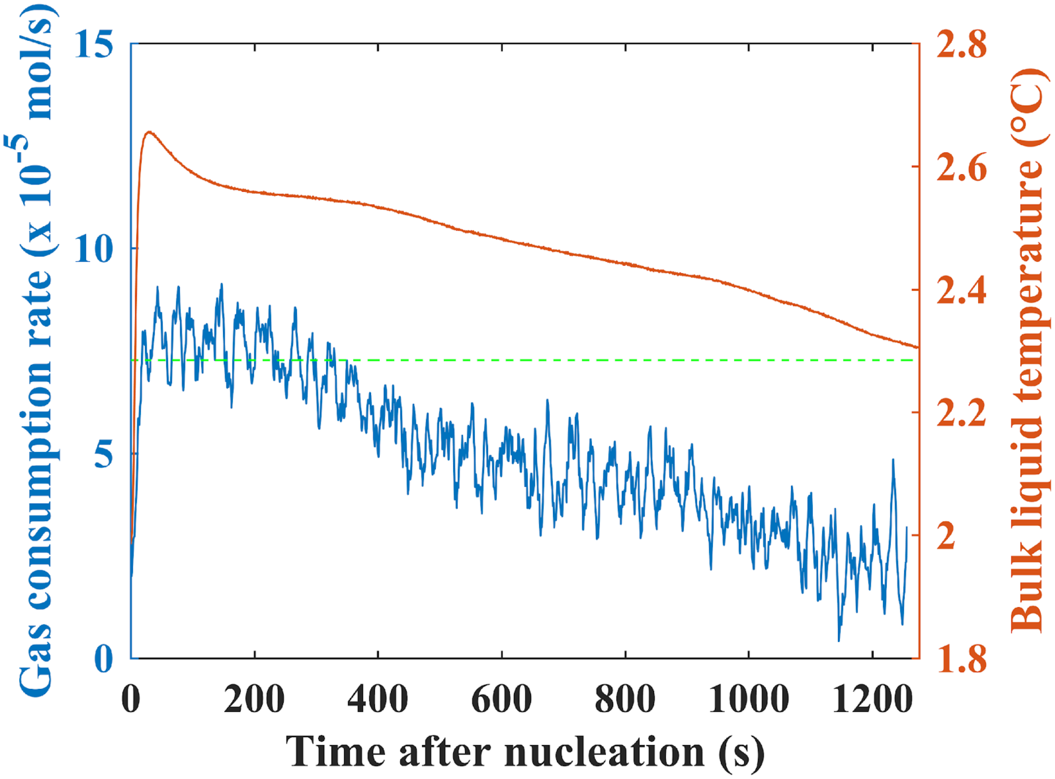

Figure 5: Instantaneous gas consumption rate (slope over a 10 second period) versus time after hydrate nucleation on the left y-axis. Dotted green line represents the 300 second average gas consumption rate. The right y-axis represents the bulk liquid temperature over time during the hydrate growth.

3.1.2 Effect of Mixing Rate

For the carbon dioxide-water gas hydrate system, the second set of experiments was completed at three different mixing rates namely 525 rpm, 560 rpm and 595 rpm. The driving force in all experiments was kept constant at 317 kPa. This driving force was selected since it had a significant variability at a mixing rate of 560 rpm as seen in Figure 3. The maximum mixing rate was set at 595 rpm since mixing rates above this speed would create gas bubbles in the liquid that would drastically change the hydrodynamics of the system. When bubbles were present in the liquid, gas consumption rates were unreliable for the experimental setup used in this study. At mixing rates lower than 525 rpm, the hydrates had very long induction times and would usually form a layer at the gas-liquid interface at nucleation as described in other reports

[29-31]. This layer significantly reduced the gas consumption rate since the gas needs to traverse a solid hydrate phase before accessing the water molecules beneath for further growth.

Gas consumption rate increases with increasing mixing rate as shown in Figure 6. Once again, the same trend where gas consumption rate decreases with increasing induction time is observed at all three mixing rates. The coefficients of variation are 3.0% (average of 3.64E-5 mol/s and standard deviation of 1.1E-6 mol/s) for 525 rpm, 9.7% (average of 6.28E-5 mol/s and standard deviation of 6.1E-6 mol/s) for 560 rpm, and 0.7% (average of 7.67E-5 mol/s and standard deviation of 5.4E-7 mol/s) for 595 rpm. A higher mixing rate seems ideal for minimizing the variability in the calculated gas consumption rates since lower mixing rates have longer induction times and more frequent hydrate layer formation. As shown by these results, the mass transfer of the gas cannot be neglected at the two lowest mixing speed because of the different average consumption rates at the highest mixing speed. It was impossible to increase the stirrer speed even higher because of low quantity of liquid used and bubble formation therefore it cannot be shown that the mass transport limitations were completely eliminated at 595 rpm. However, it is possible that the effect of induction time on gas consumption rate previously observed is not present when the mass transport limitations can be neglected.

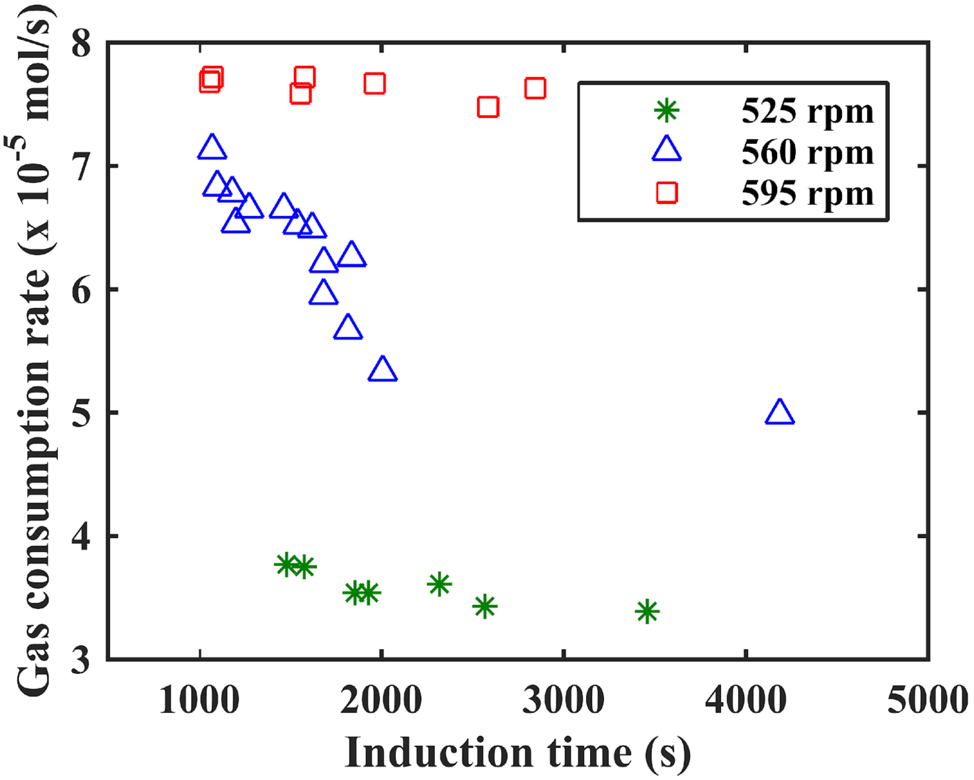

Figure 6: Gas consumption rate versus induction time for 3 different mixing rates in a CO_2-water gas hydrate system: * 525 rpm, △ 560 rpm, □ 595 rpm.

To explain the different variability in the gas consumption rates with different mixing rates, the temperature difference of the bulk liquid with induction time is analyzed. Figure 7 illustrates the dependence of the temperature spike on induction time at different mixing rates. A first-order response characterizes the relation between the variables, similarly to Figure 4. Once again, this is expected since it follows dissolution kinetics. The lowest mixing rate of 525 rpm has smaller temperature spikes than the two higher mixing rates at a similar induction time. At the lowest mixing rate, it takes longer for the same amount of gas to dissolve in the liquid than at a higher mixing rate. Mixing rates of 560 rpm and 595 rpm are not significantly different from each other with respect to their temperature spikes changes with induction time. This means that the initial amount of gas hydrates formed at nucleation for both cases are very similar. The lowest variability in gas consumption rate at 595 rpm compared to 560 rpm can be explained by the more efficient mixing since in both cases, the same amount of hydrates is present at nucleation. Gas transfer to the liquid phase in the presence of solid particles is enhanced at the highest mixing rate. This could be due to the increasing heat transfer coefficient and contact area as described in Herri et al. [28].

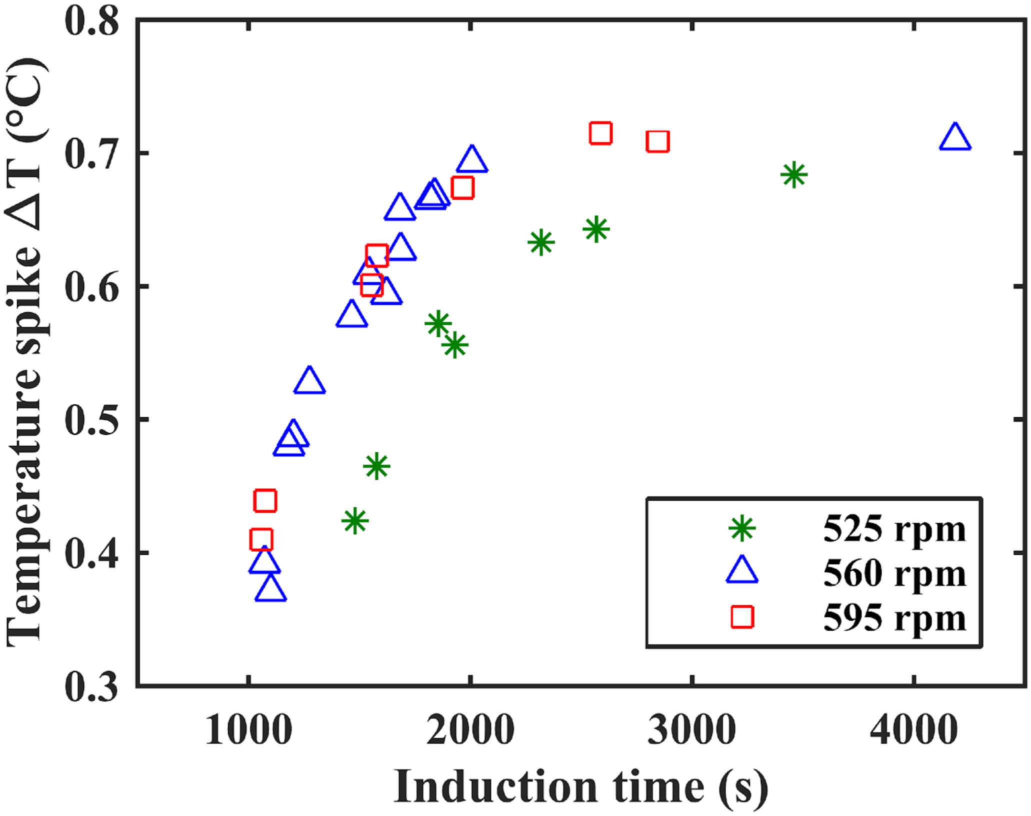

Figure 7: Temperature spike versus induction time for 3 different mixing rates in a CO_2-water gas hydrate system: * 525 rpm, △ 560 rpm, □ 595 rpm.

3.1.3. Analysis of Liquid Mole Fraction Before Nucleation

Focusing on the moles consumed before hydrate nucleation during a kinetic run, it is possible to extract information from the gas dissolution kinetics. The model presented in Equation 2 is used to regress the hypothetical maximum amount of liquid moles dissolved n_{liq}

and the time constant τ, used to designate the point in time where 63.2% of the n_{liq} is reached. The data regressed was using the CO_2 hydrate experimental runs from the previous two sections. Only the gas consumption data before hydrate formation is used for the regression. This differs from traditional dissolution results that are taken at the three-phase equilibrium conditions because the moles consumed used in the regression are taken at hydrate-forming conditions where the system is metastable. Results are presented in Table 2 with the 95% confidence intervals on each parameter. The dissolution at the same mixing rate but different driving forces has the same time constant with 95% confidence. Therefore, there is no significant difference in the amount of time to dissolve n_{liq} moles for different driving force. However, the liquid mole fraction limits are higher with greater driving force. This explains the faster nucleation and the presence of a greater initial amount of gas hydrate for the highest driving forces. Even though the time constant is the same, the mole fraction limit is greater for higher driving forces, resulting in more moles dissolved in the same amount of time. For different mixing rates, opposite trends are observed. With 95% confidence, the time constant decreases with increasing mixing rate. On the other hand, the hypothetical liquid mole fraction is not affected by the mixing rate. This means that gas dissolves faster for a higher mixing rate at the same conditions and driving forces. The mole saturation values are directly related to the driving force and do not seem to be influenced by the mixing rate, at least for the range investigated in this work. These values were compared to the number of moles dissolved at nucleation for all the carbon dioxide experiments. With 95% confidence, the values of mole saturation and mole dissolved at nucleation were the same. This means that the excess gas in the liquid can be calculated by subtracting the amount of equilibrium three-phase moles in the experimental quantity of liquid (300 mL) to n_{liq}. To use intensive properties, the mole fractions were used instead of quantity of moles for the supersaturation discussion.

Table 2: Metastable dissolution modeling parameters of all experimental conditions for CO_2 hydrates.

Pressure driving force (kPa)	Mixing speed (rpm)	τ (s)	$\tau_{95\%,lower}$ (s)	$\tau_{95\%,upper}$ (s)	n_{liq} (mol)	$n_{liq,95\%,lower}$ (mol)	$n_{liq,95\%,upper}$ (mol)
204	560	326	314	338	0.237	0.233	0.242
317	560	314	310	318	0.248	0.245	0.250
435	560	304	299	310	0.256	0.252	0.260
317	525	405	386	423	0.244	0.238	0.249
317	595	278	272	284	0.248	0.243	0.252

Figure 8 plots the liquid mole fraction supersaturation percent against the temperature difference in the bulk liquid for all the carbon dioxide experiments at all driving forces and mixing rates. Liquid mole fraction supersaturation is defined in Equation 3.

$$Liquid\ mole\ fraction\ supersaturation\ \% = 100\%\left(\frac{x^{L}-x^{HLV}}{x^{HLV}}\right) \qquad [3]$$

Where x^{L} is the calculated liquid mole fraction just before nucleation and x^{HLV} is the liquid mole fraction at three-phase equilibrium at the same temperature as the experimental condition. The baseline of 0% liquid mole fraction supersaturation corresponds to the mole fraction value from the three-phase equilibrium of carbon dioxide hydrates at 2 °C and 1574 kPa. At these conditions, the three-phase equilibrium liquid mole fraction of carbon dioxide was predicted to be 0.0161 using the model by Hashemi et al. [32] based on the thermodynamic equilibrium of gas hydrates [33, 34] and the Trebble-Bishnoi equation of state [24, 25]. The linear fit and 95% confidence intervals show that the temperature spike increases linearly with liquid supersaturation independently of the driving force and mixing rate of the system. This validates the fact that the more the system is supersaturated, the greater initial formation of gas hydrates at nucleation. Additionally, of the 46 carbon dioxide hydrate experiments, no system ever goes above 30% liquid mole fraction supersaturation. This could indicate that there is an actual experimental limit of liquid mole fraction before nucleation occurs. Contrary to spontaneous nucleation at the spinodal point [35], this experimental limit is significantly lower. For example, the spinodal limit of methane hydrates at 0.85 °C and 3290 kPa is 3.266E-2 while the equilibrium point is 1.40E-3 [35]. This results in a liquid mole fraction supersaturation that is at least 75 times greater than the thermodynamically prediction spinodal values seen in this study. Obviously, increasing the driving force will allow the potential supersaturation percent to go up, however, this would also decrease the induction time and the hydrates would form before the liquid mole fraction gets above this experimental limit. These results are characteristic of the hydrodynamics of the present experimental setup. However, it is believed that the same trend than in Figure 8 can be realized in any experimental setup. Unstirred systems would be more suitable to achieve greater liquid mole fraction supersaturation values and study this experimental supersaturation limit.

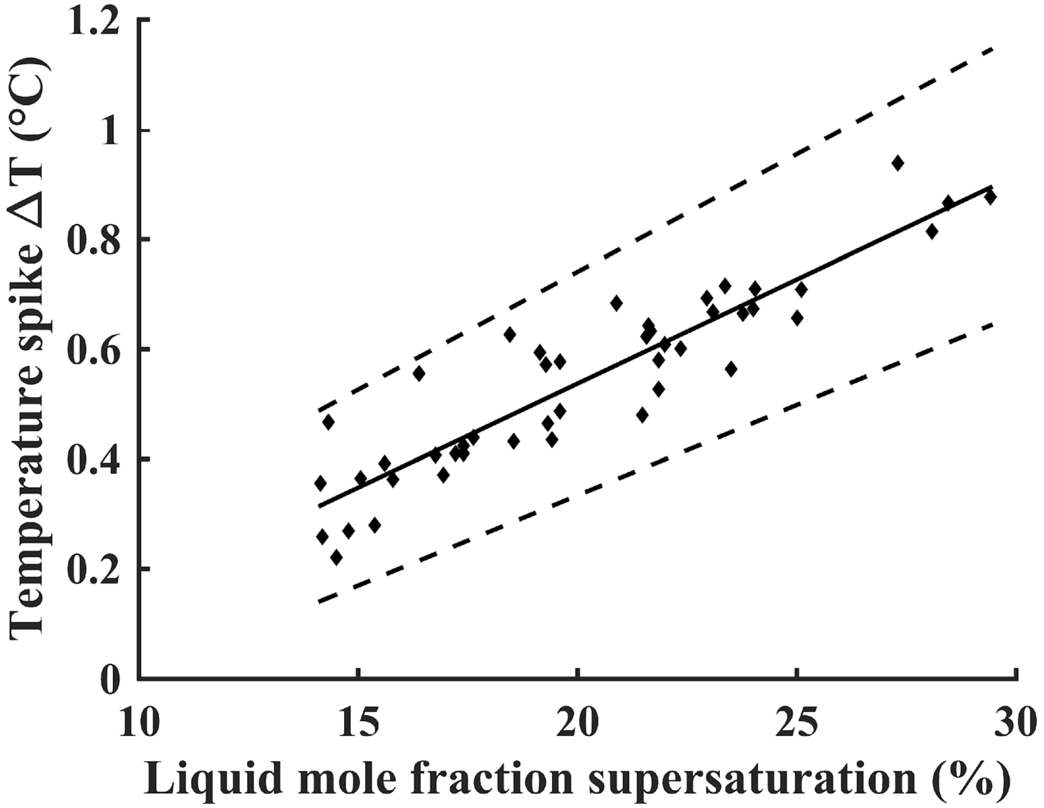

Figure 8: Temperature spike versus liquid mole fraction supersaturation of CO_2 hydrates for all experimental conditions. Data was fit with a linear trend shown by the solid line and the 95% confidence intervals shown in dotted lines.

3.2 Methane Hydrate Kinetics

3.2.1 Effect of Driving Force

The effect of induction time on methane gas hydrates is studied below. Experiments were conducted at two different driving forces, 698 kPa and 1564 kPa and the same mixing rate of 560 rpm. The conditions are displayed in Table 3. The 698 kPa driving force was selected to compare with the same temperature driving force (subcooling) as the CO_2 hydrate system while the 1564 kPa driving force was chosen because it is the same as a driving force used in previous reports [15, 36, 37].

Table 3: Two different driving force conditions for CH_4 hydrate kinetic experiments.

Temperature (°C)	Pressure (kPa)	Temperature subcooling (°C)	Pressure driving force (kPa)	Mixer speed (rpm)
2	3869	2	698	560
2	4735	4	1564	560

In Figure 9, the gas consumption rate is plotted against induction time. The decreasing trend that is evident with carbon dioxide hydrate growth is not present with methane hydrates. The coefficient of variation for 698 kPa driving force is 4.8% (average of 7.27E-6 mol/s and standard deviation of 3.5E-7 mol/s). For 1564 kPa driving force, the difference is 2.4% (average of 1.27E-5 mol/s and standard deviation of 3E-7 mol/s). Once again, it was observed that with higher driving forces came shorter induction times. This is even more apparent with methane hydrates because the induction times of different driving forces are further apart than the carbon dioxide experiments and they do not even overlap.

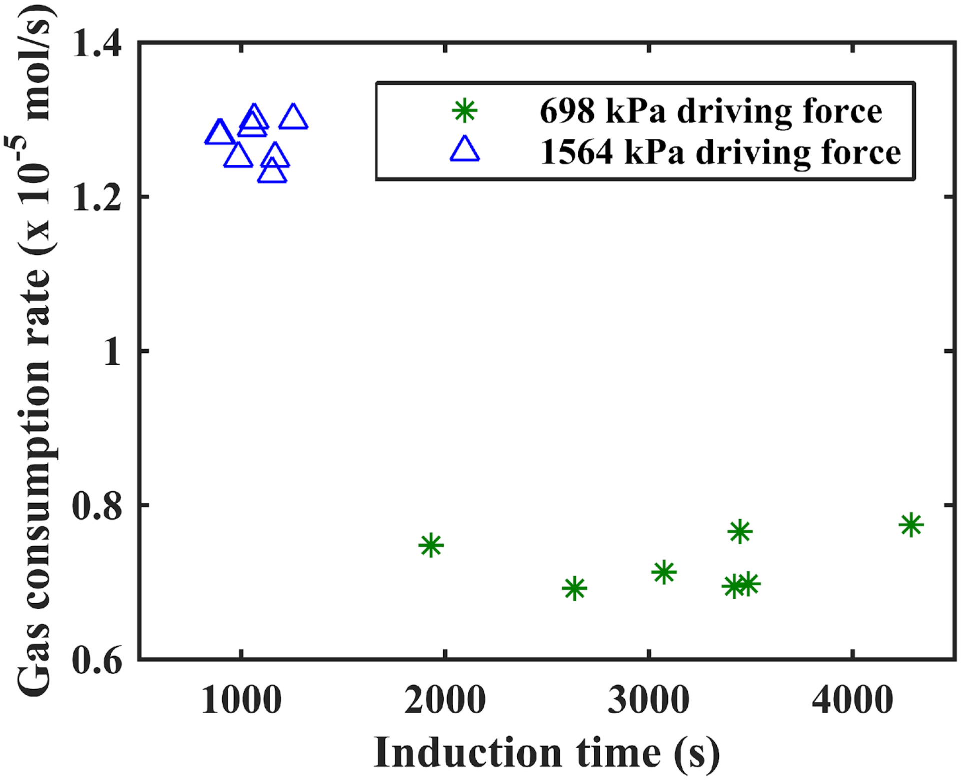

Figure 9: Gas consumption rate versus induction time for 2 different driving forces in a CH_4-water gas hydrate system: * 698 kPa, △ 1564 kPa.

Figure 10 demonstrates the dissolution kinetics of the methane hydrate system by comparing the temperature difference in the bulk liquid change with induction time. In all experiments at the 298 kPa driving force, the liquid phase had enough time to reach near its complete supersaturation state. This can be comprehended from the temperature spike measurements that are very similar. For the 1564 kPa driving force, the temperature spikes vary quite significantly but with no clear trend with the induction time. This indicates that, to the contrary of carbon dioxide gas hydrates, methane gas hydrates do not have a clear trend between the supersaturation liquid mole fraction and the temperature difference in the bulk liquid. One reason for this can be the limitation of the precision of the temperature probes being achieved. It can also be due to the fact that methane is about ten times less soluble in water than carbon dioxide. This can help explain why the supersaturation dissolution kinetics are much less important in the case of methane hydrate formation. Incidentally, the temperature spike, or initial amount of hydrates formed at nucleation, is also about ten times smaller in methane than carbon dioxide when comparing both 698 kPa driving force experiments. In sum, at these experimental conditions, it is not as crucial to study the change of gas consumption rate with induction time in the case of methane hydrates as it is with carbon dioxide hydrates. However, the trend could become apparent if the driving force and mixing rate are different, so it should remain an important consideration.

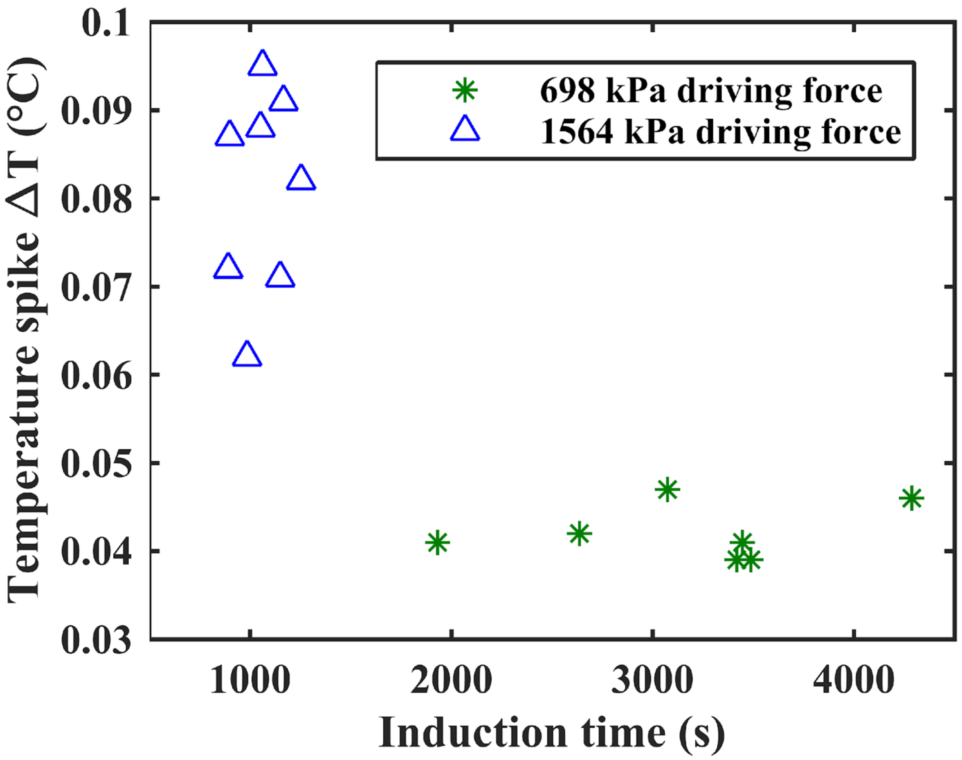

Figure 10: Temperature spike versus induction time for 2 different driving forces in CH_4-water gas hydrate system: * 698 kPa, △ 1564 kPa.

3.2.2 Discussion on mole fraction

The last part of this study investigates the liquid mole fraction during dissolution of a supersaturated methane gas hydrate system. Pure system mole fraction has been studied at the three-phase equilibrium and during the hydrate growth phase [18, 38] but not during the dissolution phase of a supersaturated system to the knowledge of the authors. An experimental run where the gas hydrate formation took a very long time was used. The mole fraction was measured when no more detectable amount of methane gas would dissolve into the liquid phase; hence it had reached complete supersaturation for the specific conditions and the gas consumption had reached a plateau. For these results, the dissolution mole fraction measurement was taken at 7450 seconds and the gas hydrates nucleated at 10 795 seconds. Shortly after nucleation, the growth phase liquid mole fraction sample was collected for comparison. It is assumed that the thermodynamically dependent mole fraction measurements are not affected by the decrease in volume in the reactor. Pressure and temperature in the system were kept constant throughout the whole experiments, including during sample extraction. The results are shown in Table 4. The three-phase equilibrium value was predicted using the model by Hashemi et al. [32] based on the thermodynamic equilibrium of gas hydrates [33, 34] and the Trebble-Bishnoi equation of state [24, 25]. The predicted three-phase equilibrium value is within the confidence interval of the hydrate growth liquid mole fraction measurement. As shown in Hashemi et al. [39], the liquid mole fraction at nucleation should be equal to its equilibrium value. They showed that the liquid mole fraction increases with time until eventually decreases towards its equilibrium with time. Verrett et al. [37] also observed the increasing trend of liquid mole fraction upon nucleation experimentally. The liquid mole fraction measurement during the dissolution phase is greater than the growth phase mole fraction with 95% confidence. Since the liquid mole fraction drops down to the three-phase equilibrium mole fraction upon hydrate nucleation, the system depends on the gas transfer to the liquid phase to start the hydrate growth. According to this explanation, for the system used in this study, the growth process would be mass-transfer limited at the gas-liquid at initial nucleation. This is a similar conclusion to the work by Skovborg et al. [40]. Eventually, as the hydrates grow and the liquid mole fraction increases, growth becomes a reaction-limited system as shown by Bishnoi and coworkers [13, 14]. These results provide additional insight on the work by Bergeron et al. [18] and the behaviour of the liquid mole fraction before and after gas hydrate nucleation at supersaturated conditions for a stirred tank reactor.

Table 4: Mole fraction of CH_4 at 2 °C and three different conditions: three-phase equilibrium at 3160 kPa, full supersaturation before hydrate formation at 3780 kPa and during hydrate growth at 3780 kPa.

	Temperature (°C)	Pressure (kPa)	x_{CH4}	$x_{CH4,95\%,lower}$	$x_{CH4,95\%,upper}$
3-phase equilibrium	2	3160	1.15E-03	-	-
Full supersaturation before hydrates	2	3780	1.25E-03	1.18E-03	1.31E-03
During hydrate growth	2	3780	1.12E-03	1.07E-03	1.16E-03

4 Conclusion

Kinetic experiments with carbon dioxide-water gas hydrates showed that the gas consumption rate decreases with increasing induction time. This is a significant finding for carbon dioxide gas hydrate studies that report a singular gas consumption rate or use this value to calculate the intrinsic kinetic rate. In all experiments, a higher driving force resulted in a shorter average induction time. The coefficients of variation on the carbon dioxide gas hydrate gas consumption rates were 2.7% for 204 kPa driving force, 9.7% for 317 kPa driving force and 9.6% for 435 kPa driving force. A high mixing rate that does not cause gas bubble formation was optimum for a smaller deviation in gas consumption rate at the same experimental conditions. For carbon dioxide hydrates, a longer induction time for these hydrates also resulted in a higher bulk liquid temperature increase at hydrate nucleation meaning a greater amount of initial hydrates formed. Methane hydrates did not exhibit the same behaviour of gas consumption rate with induction time that was observed with carbon dioxide hydrates. Coefficients of variation in gas consumption rates for methane hydrates were 4.8% for 698 kPa driving force and 2.4% for 1564 kPa driving force. Nevertheless, it was recommended to consider the trend of gas consumption rate with induction time regardless of the hydrate gas former, driving force and mixing rate. A regression of metastable dissolution during these kinetic experiments showed that the dissolution time constant decreased with increasing mixing rate. An increased driving force resulted in a greater the liquid mole fraction limit. Lastly, the maximum experimental liquid mole fraction supersaturation seen in all experiments was still 75 times smaller than the thermodynamically predicted spinodal limit.

5 Acknowledgments

The authors are grateful to the Natural Sciences and Engineering Research Council of Canada (NSERC) (grant number: 206269), les Fonds Québécois de la Recherche sur La Nature et les Technologies (FRQNT), McGill University and the McGill Engineering Doctoral Award (MEDA) for financial funding and support.

6 References

[1] E.D. Sloan, C.A. Koh, Clathrate hydrates of natural gases, CRC Press, Boca Raton, FL, 2008.
[2] P. Englezos, Clathrate hydrates, Industrial & Engineering Chemistry Research, 32 (1993) 1251-1274. DOI: http://dx.doi.org/10.1021/ie00019a001.
[3] E.G. Hammerschmidt, Formation of Gas Hydrates in Natural Gas Transmission Lines, Industrial & Engineering Chemistry, 26 (1934) 851-855. DOI: http://dx.doi.org/10.1021/ie50296a010.
[4] CBCNews, BP hits snag with containment dome, in, 2010.
[5] Y.F. Makogon, Hydrate Formation in the Gas-Bearing Layer in Permafrost Conditions, Gazovaya Promyshlennost (Gas Industry), 5 (1965).
[6] S. Thomas, Review of ways to transport natural gas energy from countries which do not need the gas for domestic use, Energy, 28 (2003) 1461-1477. DOI: http://dx.doi.org/10.1016/S0360-5442(03)00124-5.
[7] A. Eslamimanesh, A.H. Mohammadi, D. Richon, P. Naidoo, D. Ramjugernath, Application of gas hydrate formation in separation processes: A review of experimental studies, The Journal of Chemical Thermodynamics, 46 (2012) 62-71. DOI: http://dx.doi.org/10.1016/j.jct.2011.10.006.
[8] Z.-M. Xia, X.-S. Li, Z.-Y. Chen, G. Li, K.-F. Yan, C.-G. Xu, Q.-N. Lv, J. Cai, Hydrate-based CO2 capture and CH4 purification from simulated biogas with synergic additives based on gas solvent, Applied Energy, 162 (2016) 1153-1159. DOI: http://dx.doi.org/10.1016/j.apenergy.2015.02.016.
[9] I. Chatti, A. Delahaye, L. Fournaison, J.-P. Petitet, Benefits and drawbacks of clathrate hydrates: a review of their areas of interest, Energy Conv. Manag., 46 (2005) 1333-1343. DOI: http://dx.doi.org/10.1016/j.enconman.2004.06.032.
[10] N.H. Duc, F. Chauvy, J.-M. Herri, CO2 capture by hydrate crystallization – A potential solution for gas emission of steelmaking industry, Energy Conv. Manag., 48 (2007) 1313-1322. DOI: http://dx.doi.org/10.1016/j.enconman.2006.09.024.
[11] H. Dashti, L. Zhehao Yew, X. Lou, Recent advances in gas hydrate-based CO2 capture, Journal of Natural Gas Science and Engineering, 23 (2015) 195-207. DOI: http://dx.doi.org/10.1016/j.jngse.2015.01.033.
[12] Z.W. Ma, P. Zhang, H.S. Bao, S. Deng, Review of fundamental properties of CO2 hydrates and CO2 capture and separation using hydration method, Renewable and Sustainable Energy Reviews, 53 (2016) 1273-1302. DOI: http://dx.doi.org/10.1016/j.rser.2015.09.076.

[13] A. Vysniauskas, P.R. Bishnoi, A kinetic study of methane hydrate formation, Chemical Engineering Science, 38 (1983) 1061-1072. DOI: http://dx.doi.org/10.1016/0009-2509(83)80027-X.
[14] A. Vysniauskas, P.R. Bishnoi, Kinetics of ethane hydrate formation, Chemical Engineering Science Chemical Engineering Science, 40 (1985) 299-303. DOI: http://dx.doi.org/10.1016/0009-2509(85)80070-1.
[15] S. Bergeron, J.G. Beltrán, P. Servio, Reaction rate constant of methane clathrate formation, Fuel, 89 (2010) 294-301. DOI: http://dx.doi.org/10.1016/j.fuel.2009.06.019.
[16] S. Bergeron, P. Servio, Reaction rate constant of propane hydrate formation, Fluid Phase Equilibria, 265 (2008) 30-36. DOI: http://dx.doi.org/10.1016/j.fluid.2007.12.001.
[17] S. Bergeron, P. Servio, Reaction rate constant of CO2 hydrate formation and verification of old premises pertaining to hydrate growth kinetics, AIChE Journal, 54 (2008) 2964-2970. DOI: http://dx.doi.org/10.1002/aic.11601.
[18] S. Bergeron, P. Servio, CO2 and CH4 mole fraction measurements during hydrate growth in a semi-batch stirred tank reactor and its significance to kinetic modeling, Fluid Phase Equilibria, 276 (2009) 150-155. DOI: http://dx.doi.org/10.1016/j.fluid.2008.10.021.
[19] J.P. Lederhos, J.P. Long, A. Sum, R.L. Christiansen, E.D. Sloan Jr, Effective kinetic inhibitors for natural gas hydrates, Chemical Engineering Science, 51 (1996) 1221-1229. DOI: http://dx.doi.org/10.1016/0009-2509(95)00370-3.
[20] O. Söhnel, J.W. Mullin, Interpretation of crystallization induction periods, Journal of Colloid and Interface Science, 123 (1988) 43-50. DOI: http://dx.doi.org/10.1016/0021-9797(88)90219-6.
[21] H. Zhu, B.H. Shanks, T.J. Heindel, Enhancing CO−Water Mass Transfer by Functionalized MCM41 Nanoparticles, Industrial & Engineering Chemistry Research, 47 (2008) 7881-7887. DOI: http://dx.doi.org/10.1021/ie800238w.
[22] J. Pasieka, S. Coulombe, P. Servio, The Effect of Hydrophilic and Hydrophobic Multi-Wall Carbon Nanotubes on Methane Dissolution Rates in Water at Three Phase Equilibrium (V-Lw-H) Conditions, Industrial & Engineering Chemistry Research, 53 (2014) 14519-14525. DOI: http://dx.doi.org/10.1021/ie502457c.
[23] H. Bruusgaard, J.G. Beltrán, P. Servio, Solubility measurements for the CH4 + CO2 + H2O system under hydrate–liquid–vapor equilibrium, Fluid Phase Equilibria, 296 (2010) 106-109. DOI: http://dx.doi.org/10.1016/j.fluid.2010.02.042.
[24] M.A. Trebble, P.R. Bishnoi, Development of a new four-parameter cubic equation of state, Fluid Phase Equilibria, 35 (1987) 1-18. DOI: http://dx.doi.org/10.1016/0378-3812(87)80001-8.
[25] M.A. Trebble, P.R. Bishnoi, Extension of the Trebble-Bishnoi equation of state to fluid mixtures, Fluid Phase Equilibria, 40 (1988) 1-21. DOI: http://dx.doi.org/10.1016/0378-3812(88)80020-7.
[26] J. Gaudette, P. Servio, Measurement of Dissolved Propane in Water in the Presence of Gas Hydrate, Journal of Chemical & Engineering Data, 52 (2007) 1449-1451. DOI: http://dx.doi.org/10.1021/je7001286.
[27] V. Natarajan, P.R. Bishnoi, N. Kalogerakis, Induction phenomena in gas hydrate nucleation, Chemical Engineering Science, 49 (1994) 2075. DOI: http://dx.doi.org/10.1016/0009-2509(94)E0026-M.
[28] J.M. Herri, J.S. Pic, F. Gruy, M. Cournil, Methane hydrate crystallization mechanism from in-situ particle sizing, AIChE Journal, 45 (1999) 590-602. DOI: http://dx.doi.org/10.1002/aic.690450316.

[29] C.J. Taylor, K.T. Miller, C.A. Koh, E.D. Sloan Jr, Macroscopic investigation of hydrate film growth at the hydrocarbon/water interface, Chemical Engineering Science, 62 (2007) 6524-6533. DOI: http://dx.doi.org/10.1016/j.ces.2007.07.038.
[30] S.R. Davies, E.D. Sloan, A.K. Sum, C.A. Koh, In Situ Studies of the Mass Transfer Mechanism across a Methane Hydrate Film Using High-Resolution Confocal Raman Spectroscopy, The Journal of Physical Chemistry C, 114 (2010) 1173-1180. DOI: http://dx.doi.org/10.1021/jp909416y.
[31] D. Daniel-David, F. Guerton, C. Dicharry, J.-P. Torré, D. Broseta, Hydrate growth at the interface between water and pure or mixed CO2/CH4 gases: Influence of pressure, temperature, gas composition and water-soluble surfactants, Chemical Engineering Science, 132 (2015) 118-127. DOI: http://dx.doi.org/10.1016/j.ces.2015.04.015.
[32] S. Hashemi, A. Macchi, S. Bergeron, P. Servio, Prediction of methane and carbon dioxide solubility in water in the presence of hydrate, Fluid Phase Equilibria, 246 (2006) 131-136. DOI: http://dx.doi.org/10.1016/j.fluid.2006.05.010.
[33] J.H.v.d. Waals, J.C. Platteeuw, Clathrate Solutions, in: Advances in Chemical Physics, John Wiley & Sons, Inc., 1959, pp. 1-57. DOI: http://dx.doi.org/10.1002/9780470143483.ch1.
[34] W.R. Parrish, J.M. Prausnitz, Dissociation Pressures of Gas Hydrates Formed by Gas Mixtures, Industrial & Engineering Chemistry Process Design and Development, 11 (1972) 26-35.
[35] P. Englezos, P.R. Bishnoi, Gibbs free energy analysis for the supersaturation limits of methane in liquid water and the hydrate-gas-liquid water phase behavior, Fluid Phase Equilibria, 42 (1988) 129-140. DOI: http://dx.doi.org/10.1016/0378-3812(88)80054-2.
[36] J. Pasieka, S. Coulombe, P. Servio, Investigating the effects of hydrophobic and hydrophilic multi-wall carbon nanotubes on methane hydrate growth kinetics, Chemical Engineering Science, 104 (2013) 998-1002. DOI: http://dx.doi.org/10.1016/j.ces.2013.10.037.
[37] J. Verrett, P. Servio, Evaluating Surfactants and Their Effect on Methane Mole Fraction during Hydrate Growth, Industrial & Engineering Chemistry Research, 51 (2012) 13144-13149. DOI: http://dx.doi.org/10.1021/ie301931m.
[38] P. Servio, P. Englezos, Measurement of Dissolved Methane in Water in Equilibrium with Its Hydrate, Journal of Chemical & Engineering Data, 47 (2002) 87-90. DOI: http://dx.doi.org/10.1021/je0102255.
[39] S. Hashemi, A. Macchi, P. Servio, Dynamic Simulation of Gas Hydrate Formation in a Three-Phase Slurry Reactor, Industrial & Engineering Chemistry Research, 48 (2009) 6983-6991. DOI: http://dx.doi.org/10.1021/ie801674e.
[40] P. Skovborg, P. Rasmussen, A mass transport limited model for the growth of methane and ethane gas hydrates, Chemical Engineering Science, 49 (1994) 1131-1143. DOI: http://dx.doi.org/10.1016/0009-2509(94)85085-2.